JTTEE5 19:841–851
DOI: 10.1007/s11666-010-9483-2
1059-9630/$19.00 © ASM International

The Effect of HVOF Particle-Substrate Interactions on Local Variations in the Coating Microstructure and the Corrosion Resistance

Ondrej Racek

(Submitted June 2, 2009; in revised form January 4, 2010)

Splashing and redeposition of droplets occur during thermal spray processing, which affects the coating porosity and morphology. Therefore, this phenomenon is important from a practical point of view such as corrosion. Particle interaction with substrate is a function of the particle velocity, viscosity, temperature, as well as the substrate temperature, chemistry, roughness, and geometry. In the present study, the splashing phenomenon was studied on CrC-NiCr and stainless steel materials deposited using the high velocity oxygen fuel process. The effect of particle splashing on the coating microstructure was investigated with respect to the corrosion properties. Particle behavior during impact was explained based on in-flight particle velocity and temperature measurements. It was found that the conditions that favor particle splashing promote occurrence of localized porosity. The localized porosity was a strong function of the substrate curvature and originated from the substrate asperities.

Keywords cermet coatings, corrosion, HVOF microstructures, HVOF spray parameters

1. Introduction

HVOF technology is used to deposit coatings for wear and corrosion protection due to its ability to form a dense deposit compared to other processes in ambient atmosphere (Ref 1). HVOF coatings are used as replacement of hexavalent chromium on hydraulic cylinders such as actuators and struts (Ref 2) or printing rolls (Ref 3). Due to the complex nature and many varieties of wear, there may (Ref 4) or may not (Ref 5) be a clear correlation between the hardness and the wear resistance under particular service conditions. However, generally coating porosity decreases the hardness and the elastic modulus (Ref 4, 6, 7). Coating density is also important for the corrosion protection especially if the coating is cathodic with respect to the substrate (Ref 8, 9). Open porosity in the coating allows the electrolyte to penetrate to the anodic substrate that would be attacked by localized galvanic corrosion.

Typically coating porosity decreases and hardness increases with increasing particle velocity (Ref 5, 10) due to a stronger peening effect. However, high particle velocity may also be associated with higher degree of particle splashing that has detrimental effect on coating density and adhesion (Ref 11). Localized porosity and high oxide content can be formed due to redeposition of splashed metallic particles. Redeposition of splashed particles on walls of a deep notch was observed during wire arc spray deposition (Ref 12). It was also shown that the substrate geometry affects the flow of impacting and splashed particles. Buildup of splashed particles around perturbations on otherwise smooth surfaces was observed under plasma spray conditions (Ref 13).

A significant amount of research has been dedicated to investigation of the splashing phenomena. Impact

List of Symbols	
K	Sommerfeld parameter
K_f	modified Sommerfeld parameter
We	Weber number
Re	Reynolds number
ρ	particle density
d_0	particle diameter prior to impact
V	particle velocity prior to impact
V_f	particle flattening velocity
σ	surface tension
μ	viscosity
a	ratio of the flattening and impact velocity
T_s	substrate temperature
$\phi = \frac{n_{fuel}/n_{oxidizer}}{(n_{fuel}/n_{oxider})_{st}}$	equivalence ratio
n_{fuel}	number of moles of fuel
$n_{oxidizer}$	number of moles of oxidizer
SOD	standoff distance
DE	deposition efficiency

Ondrej Racek, Caterpillar, Inc., Peoria, IL. Contact e-mail: racek_ondrej@cat.com.

splashing of liquid droplets is governed by Sommerfeld parameter (Ref 14):

$$k = \sqrt{We \cdot \sqrt{Re}} = \frac{(\rho \cdot d_0)^{\frac{3}{4}} \cdot V^{\frac{5}{4}}}{\sigma^{\frac{1}{2}} \cdot \mu^{\frac{1}{4}}} \quad \text{(Eq 1)}$$

where We, Re, ρ, d_0, V, σ, and μ are the Weber number, Reynolds number, particle density, the initial diameter, the particle velocity, the surface tension of the air-liquid interface, and the viscosity. Increasing the Sommerfeld parameter increases the tendency for particle splashing. Higher kinetic energy results in a stronger tendency to splashing. On the other hand, viscosity dissipates the kinetic energy on impact and together with surface tension act against particle splashing. Rayleigh-Taylor instability of a fluid accelerating into a denser fluid has been suggested as a possible mechanism of splat ''fingering'' (Ref 15).

Particle splashing is influenced not only by the in-flight particle properties prior to impact but also other factors such as substrate wetting by the particle material, substrate roughness, adsorption of gases and condensation on the substrate, particle solidification or even localized substrate melting (Ref 16). Splashing that occurs due to interaction with the substrate during splat formation is termed flattening splashing in (Ref 17).

For example, splashing can be suppressed if the substrate temperature, T_s, is higher than a transition temperature, T_t (Ref 18). Transition temperature increases with increasing the substrate thermal conductivity (Ref 19). Smaller grains were observed at the bottom of the central part of splashed Ni splats deposited on a substrate below T_t compared to disk-shaped splats deposited at temperatures over T_t (Ref 19), which indicated higher cooling rate occurred at the bottom of the splats splashed on the substrate at low temperature. On the other hand, the splashed splats deposited at temperatures below T_t exhibit porous microstructure at the interface with the substrate that effectively forms a thermal barrier against cooling of the rest of the solidifying particle (Ref 20). Direct time-resolved observation of plasma-sprayed zirconia particle temperature after impact (Ref 21) showed that the cooling rate of disk-shaped splats, deposited on substrates at $T_s > T_t$, is significantly higher than the cooling rate of splashing splats deposited on substrates at $T_s < T_t$. Higher splat cooling rate at $T_s > T_t$ occurred due to better wetting between the particles and the substrate (Ref 22). Larger grains within copper splats were observed when $T_s < T_t$ due to slower solidification that resulted from increased thermal resistance at the splat-substrate interface. Increase of the transition temperature with increasing the substrate thermal conductivity (Ref 18), which makes splashing easier to occur, is therefore not related to an increase of the splat overall cooling rate but promotes faster solidification at the splat-substrate interface. Faster solidification at the interface may increase the amount of pores that, in turn, slow down solidification of the rest of the particle.

Flow instabilities that result in particle splashing may also be caused by surface asperities (Ref 19) or by solidification of a part of the particle before splat formation is finished (Ref 21). A model of splat splashing has been suggested (Ref 19) that is consistent with the experimental observations. In the model, a thin porous layer of solidified material is formed at the bottom of the central part of a splat that impedes the particle cooling and liquid flow. The liquid on top of the thin solid layer is then ejected further away from the splat center. Under non-splashing conditions, improved wetting between the particle and the substrate promotes efficient dissipation of kinetic energy by viscosity and the solidification occurs more uniformly (Ref 19).

A modified Sommerfeld parameter has been proposed that is based on the splat flattening velocity and the splat thickness rather than on the in-flight particle velocity and diameter (Ref 17, 23):

$$K_f = 0.5 \cdot a^{1.25} Re^{-0.3} K \quad \text{(Eq 2)}$$

where K is the Sommerfeld parameter based on the particle impact velocity and diameter prior to flattening (1) and a relates the impact velocity V to the maximum flattening velocity V_f:

$$V_f = aV \quad \text{(Eq 3)}$$

The modified criterion for splashing includes the effect of substrate temperature and the critical value was estimated from measurements of free falling nickel droplets (Ref 23) to be about 6. However, the ratio of the flattening and the impact velocities a has to be determined experimentally.

Other factors of practical importance that affect particle splashing include substrate roughness, oxidation, adsorbed gases, and impact angle. Although splats are more distorted when impacting on rough surfaces and the flattening ratio tends to be lower (Ref 21), roughness is typically needed to achieve sufficient coating adhesion (Ref 24). Splat cooling rate is controlled, among other factors, by its thickness; therefore, the observation of smaller flattening ratio is consistent with increasing cooling time of molybdenum particles when increasing roughness of glass or molybdenum substrates (Ref 25). It has been shown that the average cooling rate of molybdenum particles as a function of substrate roughness has a minimum and the cooling rate increases above this minimum due to a larger effective contact area (Ref 26). Excessive substrate oxidation has impact on wetting properties of the substrate and can cause splashing even if $T_s > T_t$ (Ref 21). However, some results indicate that preheating at $T_s > T_t$ forms a few nanometers thick oxide layer, which improves the surface wettability due to an increase in surface profile skewness at the nanometer scale (Ref 27). Other results suggest that the wetting behavior is modified also due to changes in nanometer-scale surface roughness induced by heating in the absence of oxidation (Ref 28). Ambient pressure has a strong effect on T_t and particle splashing can be suppressed at low pressures (Ref 20). There is a significant amount of evidence that the particle splashing is at least partially caused by gases/vapor adsorbed or condensed on the substrate surface (Ref 27-29).

Plasma sprayed particles have probably been studied most extensively with respect to the splashing behavior;

however, the splashing phenomenon is relevant also for other types of coating techniques. The substrate temperature has been found to be a strong factor in particle splashing under wire arc spray conditions (Ref 30). In both plasma and arc spray, most particles are fully molten prior to impact whereas the HVOF particles are frequently only partially molten or even solid (Ref 31). Under HVOF or high velocity air-fuel spray (HVAF) conditions, partially molten or softened particles are plastically deformed and the kinetic energy is converted into additional heat. HVOF and HVAF sprayed particles can undergo splashing similar to the plasma sprayed particles (Ref 32). Although the HVOF splat formation cannot be described exactly in the same fashion as the plasma splats, the relation of the splashing tendency to the particle velocity and viscosity (2) might be similar. Analysis of the splashing phenomenon is further complicated if heterogeneous particles such as CrC-NiCr cermets are used. In the present study, no attempt was made to analyze the event of an individual particle splashing but rather the effect of splashing on the coating microstructure was studied from a practical point of view.

Since previous experiments indicated that the trajectory of splashed particles might be affected by the size or geometry of the substrate, flat and cylindrical specimens were used in the present study to investigate the effect of the surface curvature. This effect is practically important; for example a strut of a large mining truck is about 400 mm in diameter, which is significantly less curved surface than hydraulic cylinders for small actuators that may be only about 40 mm in diameter. In addition to the effect of splashed particles, off-angle spraying may lower the coating hardness and increase porosity (Ref 33, 34). In the present study, the deviation of a particle trajectory from the surface normal due to the curvature would not exceed about 13 degrees since the particle stream width was small, about 20 mm, compared to the cylinder diameter, 90 mm. Therefore, the effect of the particle impact angle on the coating porosity was considered negligible. During coating deposition, cylindrical parts are typically rotated about the axis and the thermal spray torch traverses along the axis. Since the particle velocity is at least two orders of magnitude higher than the velocity of the surface with respect to the torch, the rotation effect on the resultant particle velocity relative to the substrate and the impact angle is negligible.

Equivalence ratio Φ (the ratio of the actual fuel to oxygen ratio and the stoichiometric ratio) and the standoff distance were other parameters in the present study since they significantly influence the in-flight particle temperature and velocity. Although no direct observation of particle splashing was performed, microscopic observation of splashed or fragmented particles deposited within coatings or on polished steel substrates provided a link between the coating properties and particle splashing behavior. HVOF coatings are frequently applied on steel components that have been heat-treated; therefore, it was not practical to investigate the effect of T_t on the coatings microstructure since high temperature would excessively temper the steel.

2. Experimental Procedures

Spray-dried sintered CrC-NiCr (Sulzer Metco WOKA GmbH, Barchfeld, Germany) and water atomized 316L stainless steel (Hoeganaes, Cinnaminson, NJ) powders were deposited using a JP 5000 kerosene fueled torch (Praxair Surface Technologies TAFA Incorporated, Concord, NH, USA). Particle velocity and temperature were measured using the Accuraspray instrument (Tecnar, St. Bruno, Canada), which uses cross-correlation of two intensity signals to measure the particle velocity and two-color pyrometry to measure the temperature (Ref 35).

The coatings were deposited low carbon steel substrates that were either flat plates (F), 203 by 102 mm, or cylinders (C) 305 mm long and 90 mm in diameter. All specimens were grit-blasted prior to coating deposition and the substrate roughness was approximately $R_a = 8$ μm. During coating, the cylinders were rotated at 213 RPM and the torch was moved along the axis using a robot at a speed of 21.3 mm/s. The torch was aligned perpendicular to the cylinder surface using a laser pointer. To coat the plates, the torch was moved in a raster pattern with traverse speed of 1000 mm, i.e., speed equivalent to the cylinder surface speed relative to the torch, and the raster step was 6 mm, which was the same distance that the torch footprint travelled on the cylinders during a single revolution. Substrates were not preheated prior to deposition and air-cooling was used such that T_s did not exceed 150 °C. Powder feedstock was injected radially at two locations 180° apart immediately before a 101.6 mm long straight barrel. Each injector was fed from a separate powder feeder and the total feedrate was 96 g/min.

The experimental factors and their levels are listed in Table 1 and 2. For deposition of the CrC-NiCr, two gas flow settings were selected such that the average particle speeds at a given standoff distance were approximately the same and the equivalence ratio was either low or high, Table 2. The maximum flame temperature at a given pressure would occur at an equivalence ratio higher than one due to dissociation (Ref 36). The total mass flow of oxygen and kerosene had to be set higher for the lower equivalence ratio to reach the same velocity, which is consistent with the particle temperature and velocity measurements for the conditions T3 and T6 in (Ref 5). The average particle velocity decreases as a function of the standoff distance (SOD) and the average particle temperature follows the opposite trend, Fig. 1. Note that the lengths of the error bars in Fig. 1 are twice the standard deviation estimated from approximately 130 individual measurements. The error bars for the velocity

Table 1 Experimental conditions for CrC-NiCr deposition

Factors levels	SOD, mm	Equiv. ratio Φ	Substr. radius, mm
Low	279	0.99	45 (C)
Med	305	…	…
High	330	1.16	∞ (F)

Table 2 Oxygen and fuel flow details

	K1 flow, lph	O_2 flow, slpm	Equiv. ratio Φ	Mass flow, g/min	Carrier gas (N_2) flow, slpm
CrC-NiCr	27.3	806	1.16	1524	6.1
	24.8	860	0.99	1567	6.1
316L	23.2	806	0.99	1468	7.0

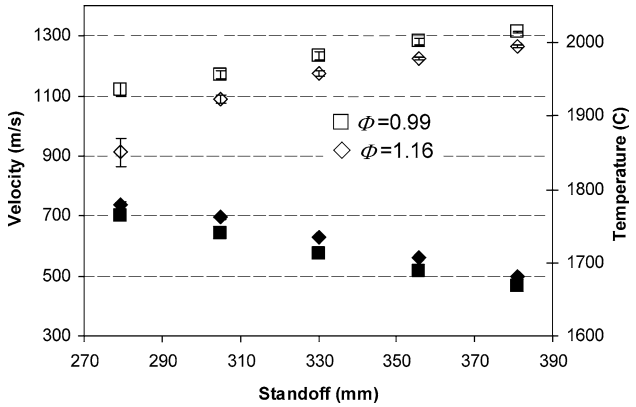

Fig. 1 Particle velocity and temperature data for the CrC-NiCr powder 15-75 μm particle size

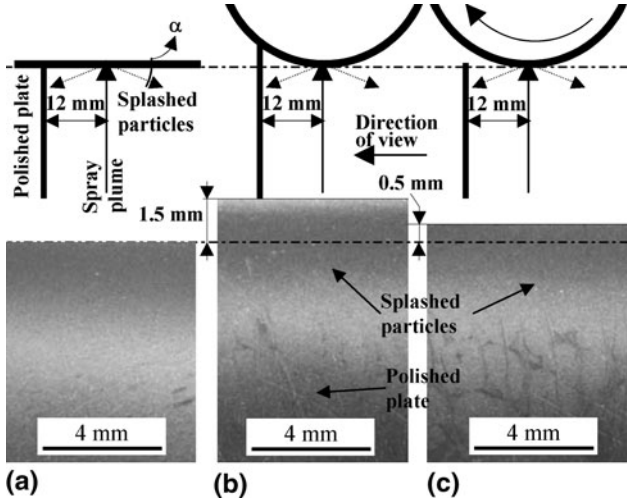

Fig. 2 Perpendicular polished plates used to collect splashed particles; the setup schematics and images of the surfaces after exposure to splashing particles: (a) plate, (b) stationary cylinder, (c) rotating cylinder (the plate edge ~0.5 mm from the surface)

measurements are smaller than the data point symbols. Each individual measurement lasted about one-second and its value represented the average of all particles that contributed to the detected signal. The in-flight temperature measurements indicated a lower particle temperature at a higher equivalence ratio, which contradicted the expectation of a higher flame temperature.

Processing of the 316L stainless material was limited to only one parameter, Table 2, since other parameters that were tested resulted in a rapid buildup of the coating material on the inside diameter of the torch barrel. The buildup disturbed the gas flow and caused a drop in the particle velocity that was typically detected by the in-flight diagnostic equipment even before a visible change in the plume occurred. The buildup is frequently caused by excessive amount of fine particles in the feedstock; therefore, the 316L material was screened to remove particles less than 20 μm in diameter. The 316L material was deposited at 305, 330, and 356 mm standoff.

Cross sections of coating specimens were polished using diamond abrasives. Microstructure of the cross sections was examined with respect to redeposition of splashed particles. Additionally, splashed particles were collected on polished steel plates, 20 by 80 mm that were placed close to the spot where the HVOF plume impinged on planar or cylindrical grit-blasted surfaces. The centerline of the HVOF plume passed close to the plates at a speed of 1000 mm/s parallel to their planes and at a distance of 12 mm above the polished surface, Fig. 2. Laser pointer aligned with the HVOF plume was used to align the path of the torch, attached to a robot, with the polished plates and the grit-blasted substrates. The plates were perpendicular to the substrate plane or to the tangent at the point of impact. Three cases were examined; (a) stationary plate, (b) stationary cylinder, and (c) rotating cylinder. Note that the edge of the polished plate did not make contact with the surface of the rotating cylinder and the edge was about 1 mm away from its surface; therefore, the particles splashed at an angle directed immediately above the substrate surface could be collected only in the cases of the stationary cylinder and the plate.

Hardness and elastic modulus were measured using a MHT depth-sensitive indentation instrument (CSEM, Neufchatel, Switzerland) and a computerized AMH43 microhardness tester (LECO, St. Joseph, MI) that uses optical measurement of the indent size. All hardness measurements were performed at 300 g load and the indents were placed in an equidistant array with 100 μm spacing. The mechanical properties in some areas of interest were mapped in arrays using equidistant spacing of 62 μm. The spacing was selected such that the diagonal of an indent that was representative of the average coating hardness would be about 2.5 times smaller than the array spacing, a practice described in the ASTM standard E 92 for testing of metallic materials. However, some indents, especially in the porous areas, were as large as about 50% of the array spacing. Therefore, the shorter spacing may have had effect on some indentations; nevertheless, the shorter spacing was used since the purpose of the mapping was to document only the relative variation of mechanical properties within the microstructure and not to obtain a certified hardness value. Using lower load, on the other hand, would result in smaller indents so the spacing would have less effect on the measurement; however, small indents within the heterogeneous coating structure would be more difficult to measure and the measurements would be more affected if indentations coincide with pores.

The load-displacement curve can be analyzed to estimate the indenter contact area, which together with the initial unloading contact stiffness yields the elastic modulus (Ref 37). In the present study, the elastic modulus was estimated based on the stiffness and the contact area that was measured optically using the AMH43 hardness tester.

The corrosion resistance of the coatings was qualitatively compared by the amount of red rust on the surface after a continuous exposure to a salt fog (ASTM B117). The coatings were tested in the as-sprayed condition.

3. The Effect of the Process Parameters on the Coating Surface Morphology, Microstructure, and Deposition Efficiency

Macro roughness features—speckles—were formed when parameters associated with higher particle velocities and higher equivalence ratios were used. The particle velocity was a strong function of the standoff distance over the 51 mm range. Under the high equivalence ratio condition, Table 1, the speckles formed on CrC-NiCr coatings extensively at 279 mm standoff. A representative sample of such coating surface, Fig. 3a, was recorded using a digital microscope, VHX-600 (Keyence, Osaka, Japan), capable of digital depth composition. The effect was less obvious at 305 mm and completely disappeared at 330 mm, Fig. 3(b) and (c). No macro roughness features were formed under the low equivalence ratio condition at all standoff distances. Similar speckles were formed on 316L coatings at 305 and 330 mm standoff and the effect disappeared at 356 mm standoff, Fig. 3(d).

The speckles, having a highly porous microstructure, appeared to grow during the coating deposition in a conical shape that often originated at a substrate protrusion, Fig. 4(a). The speckle microstructure consisted of small highly oxidized particles, Fig. 4(b); the rest of the coating was built up by relatively larger splats with oxides at the splat boundaries, Fig. 5. The excessive oxidation likely occurred after splashing due to high specific surface area of the small particles. Under conditions that did not favor the speckle growth, porosity could be formed at a protrusion initially; however, at a later stage a typical coating morphology with no macro roughness features covered the defective microstructure, Fig. 6(a). The porosity on the side of a protrusion under non-speckle conditions, Fig. 6(b), is similar to the porosity of a macro speckle, Fig. 4(b) except the effect that formed the excessive porosity faded soon. The oxidized particles that formed the porous microstructure were similar to the splashed particles deposited on polished steel plates, Fig. 7.

The amount of particles splashed from the flat grit-blasted substrate and deposited on the polished plate decreased with increasing the splashing angle α, Fig. 2(a), i.e., with increasing distance from the surface, Fig. 7. The splashing patterns from the rotating and stationary cylinders were both moved toward the substrates, Fig. 2(b) and (c); however, the overall amount of redeposited particles

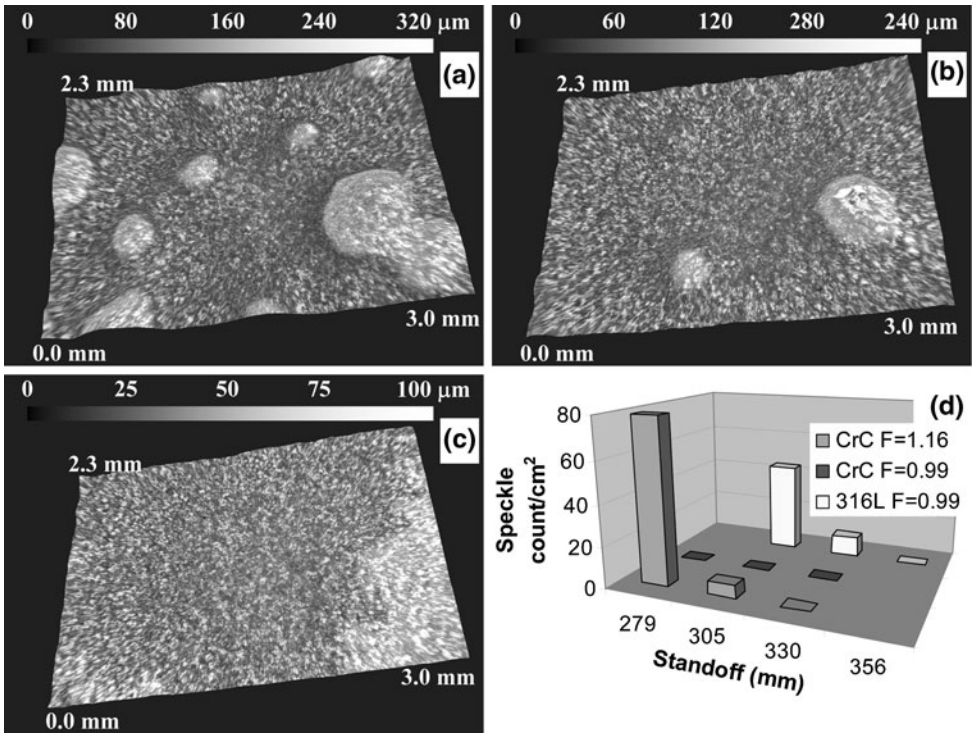

Fig. 3 The effect of standoff distance on the CrC-Ni coating surface profile (a) 279 mm, (b) 305 mm, (c) 330 mm, and (d) density of speckles with height over 100 μm

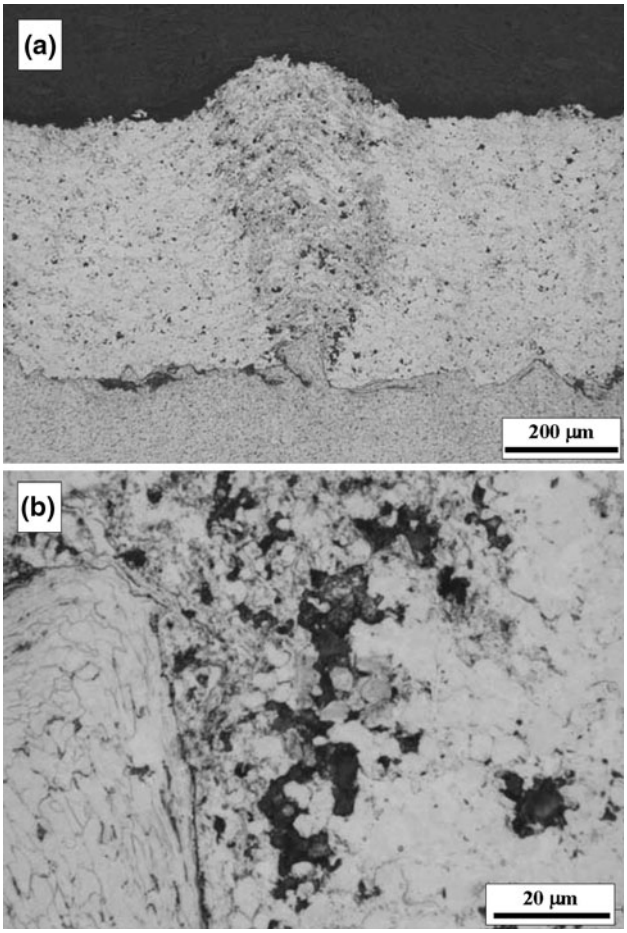

Fig. 4 An optical micrograph of the cross section of a CrC-Ni HVOF coating; (a) a porosity speckle emanating from a substrate protrusion, (b) detail of the particles deposited on the protrusion side

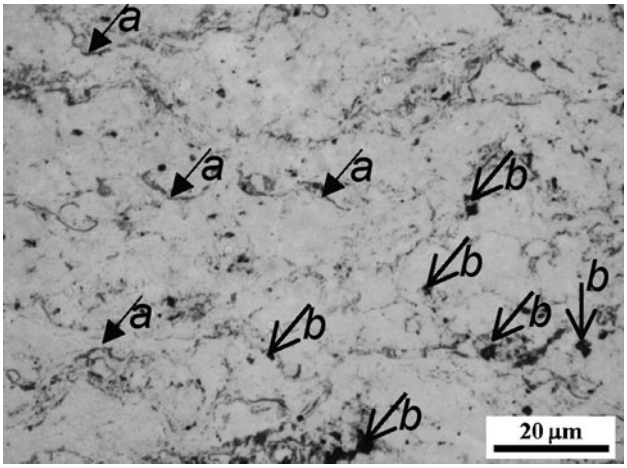

Fig. 5 An optical micrograph of a typical HVOF CrC-Ni HVOF coating morphology observed outside the areas of speckles; (a) splat boundaries oxides and (b) voids

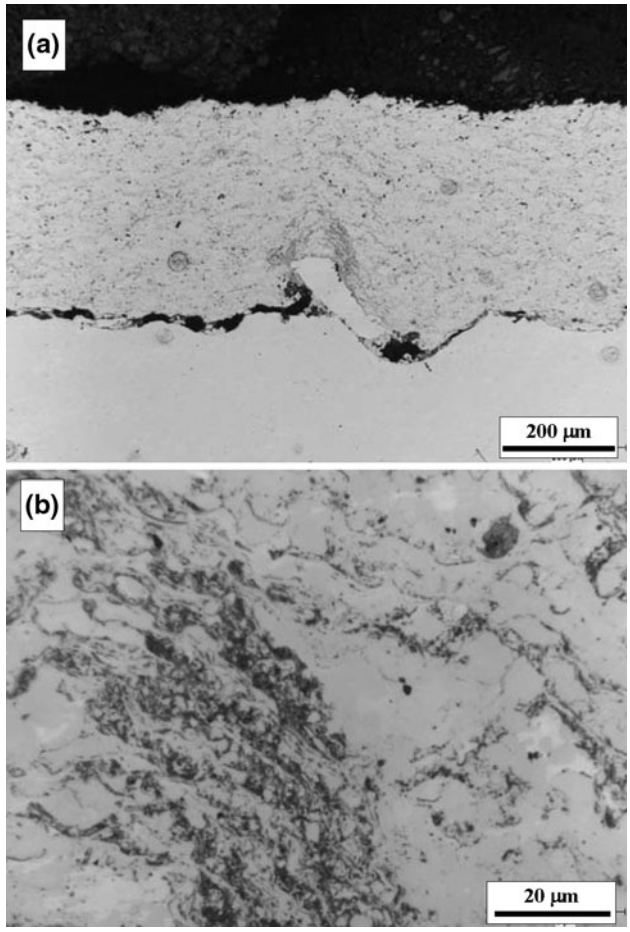

Fig. 6 Porosity in a CrC-NiCr coating formed around a substrate protrusion; (a) a relatively smooth coating that covers the defective microstructure, (b) detail of the oxidized redeposited droplets

appeared to be similar among the three configurations. There were splashed particles deposited below the tangent of the stationary cylinder; however, the amount of splashed particle decreased closer to the substrate, Fig. 7. The polished plate used to collect splashed particles from the rotating cylinder did not cover most of the zone under the tangent since the plate had to be set back to avoid contact with the rotating surface.

The deposition efficiency (DE) was higher when the higher equivalence ratio was used, Fig. 8, which would be typically expected since the adiabatic flame temperature is higher. Note that the error bars represent uncertainty estimates that were calculated from the uncertainties of measurement of the quantities that were used to calculate the deposition efficiency, i.e., the target weight, dimensions, and the powder feed rate. The standard deviation of the powder feed rate was determined in a separate experiment by recording the powder hopper weight and the time. The DE increased with decreasing standoff distance under the high equivalence ratio condition, which

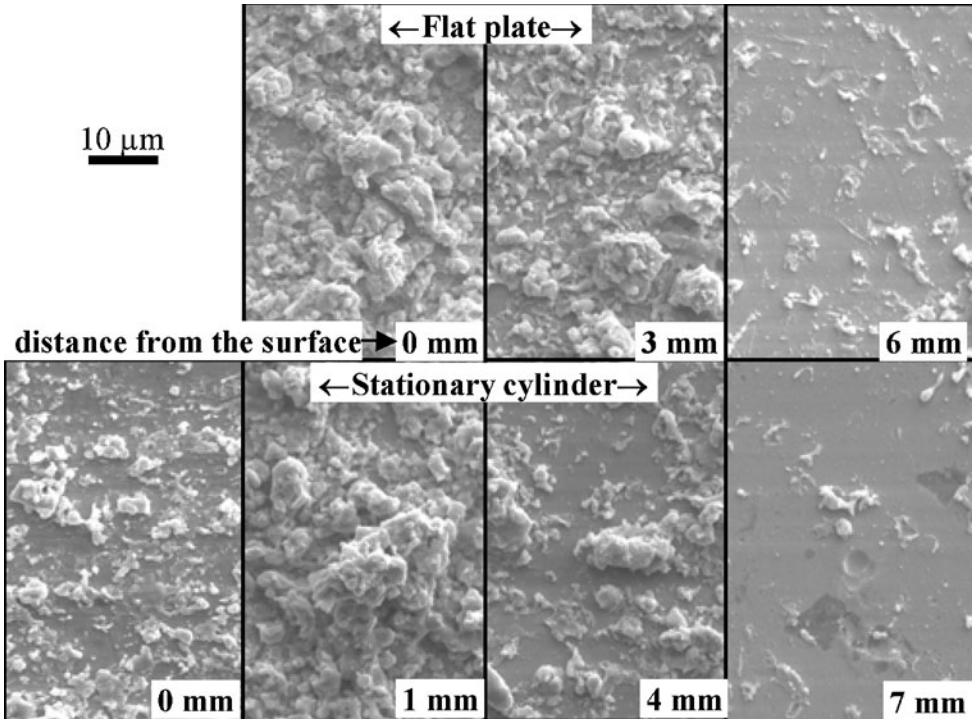

Fig. 7 The effect of distance from the substrate surface on the splashed particles deposited on polished plates observed using SEM

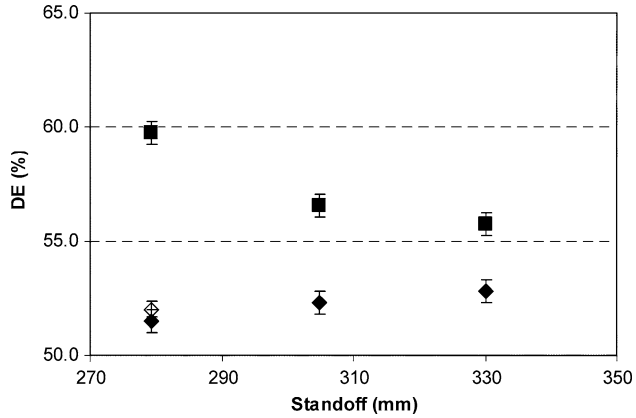

Fig. 8 CrC-NiCr deposition efficiency as a function of the standoff distance

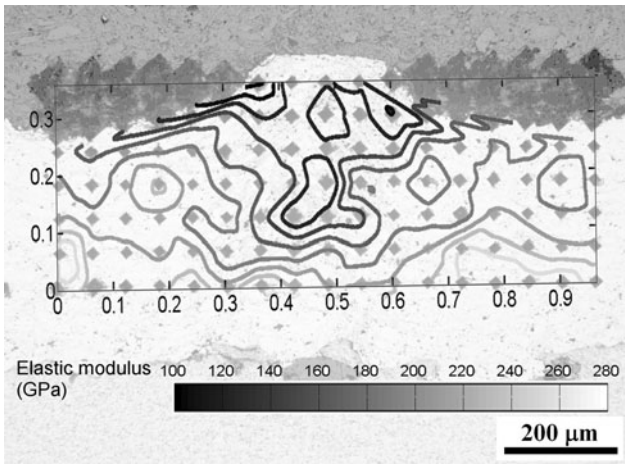

Fig. 9 Lower elastic modulus over the area of a speckle

indicated that the mass of splashed particles that form the speckles contributed to the higher DE. Under the low equivalence ratio condition the DE increased with increasing SOD.

4. The Effect of the Process Parameters on the Mechanical Properties

The porous and oxidized microstructure within the speckles had an impact on the hardness and the elastic modulus. Both the elastic modulus and the hardness were lower within the region of porous oxidized microstructure, Fig. 9. The coating integrity within the speckles was low and the loosely bonded particles were pulled out during grinding, Fig. 10.

The speckles exhibited extremely variable hardness between 120 and 1100 HV300; however, the hardness measured only outside the speckles was in the same range as the speckle-free coatings, Fig. 11. Therefore, it appears that the poor integrity of these coatings was concentrated only in the regions of speckles. It should be noted that speckles under the polished plane of the samples might have affected some indents. The coatings deposited on the

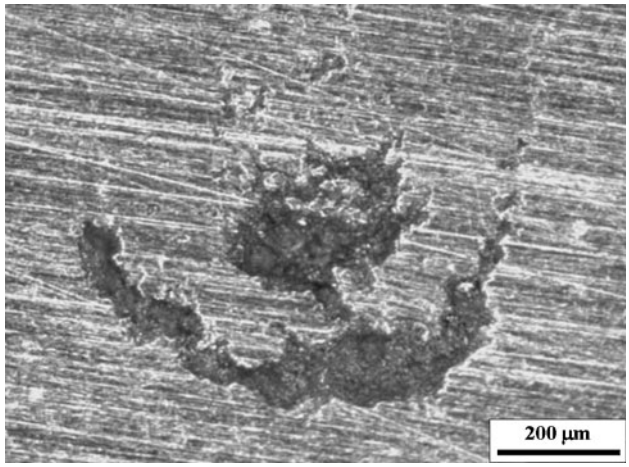

Fig. 10 Ground CrC-NiCr coating surface over a speckle, Φ = 1.16, 15-75 μm particle size, 279 mm standoff

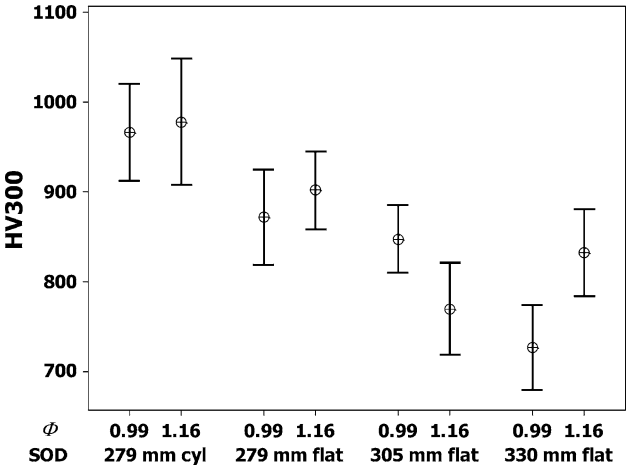

Fig. 11 Interval plot of HV300 hardness for CrC-NiCr coatings

cylindrical surfaces possessed higher hardness that the coatings deposited on the flat surfaces.

5. Corrosion Resistance

The coatings were inspected after a 24 h salt fog exposure. The coatings were qualitatively compared by the amount of red rust on the surface, Fig. 12 where the level of speckles is noted as a number of speckles that are higher than 100 μm. The coatings with speckles were corroded the most, Fig. 12(b(2)). Although the coatings without speckles performed significantly better, the red rust was present almost on all specimens.

Unlike the CrC-NiCr coatings there was little difference in the corrosion patterns of the 316L coatings, Fig. 13. Both the coating with speckles, Fig. 13(b), and the speckle-free coating, Fig. 13(d), had a significant amount of red rust. The leave-like pattern on the corroded 316L coated specimens is due to the flow pattern of the rust

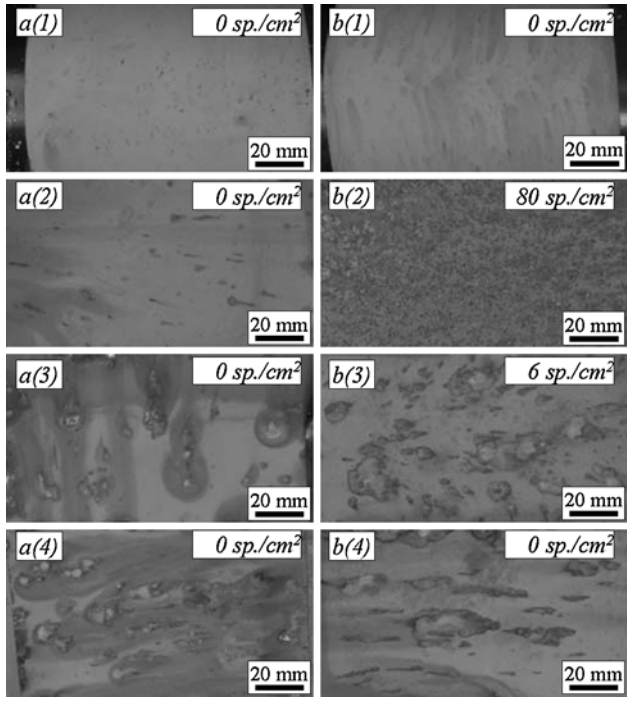

Fig. 12 CrC-NiCr coatings deposited on cylindrical (C) and flat (F) surfaces under various SOD and equivalence ratio conditions after 24 h salt fog exposure: (a(1-4)) Φ = 0.99, (a(1)) 279 mm C, (a(2)) 279 mm F, (a(3)) 305 mm F, (a(4)) 330 mm F; (b(1-4)) Φ = 1.16, (b(1)) 279 mm C, (b(2)) 279 mm F, (b(3)) 305 mm F, (a(4)) 330 mm F

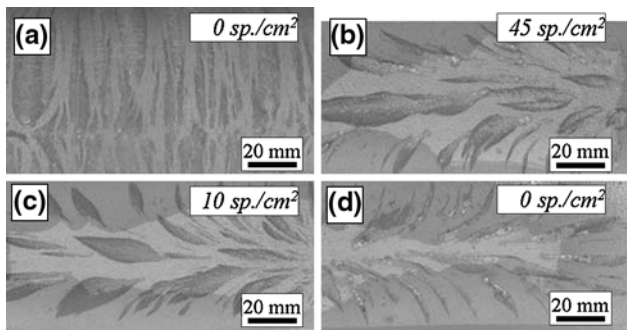

Fig. 13 As-sprayed 316L coatings deposited on cylindrical (C) and flat (F) surfaces at various SOD after 24 h salt fog exposure: (a) 305 mm C, (b) 305 mm F, (c) 330 mm F, and (d) 356 mm F

from corrosion pits. The plate specimens were tilted at 30 degrees and rust pattern was opening toward the bottom; for example the right side of the plate in Fig. 13(c) was up while the right side of the plate in Fig. 13(d) was at the bottom.

6. Discussion

Microstructural analysis of the macro-rough coatings revealed that the speckles often originated at a substrate

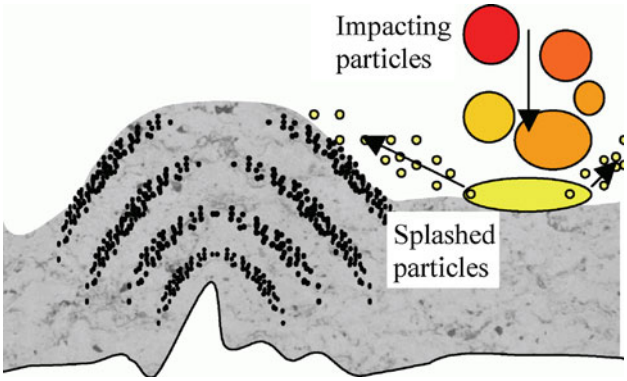

Fig. 14 Suggested mechanism of the speckle formation

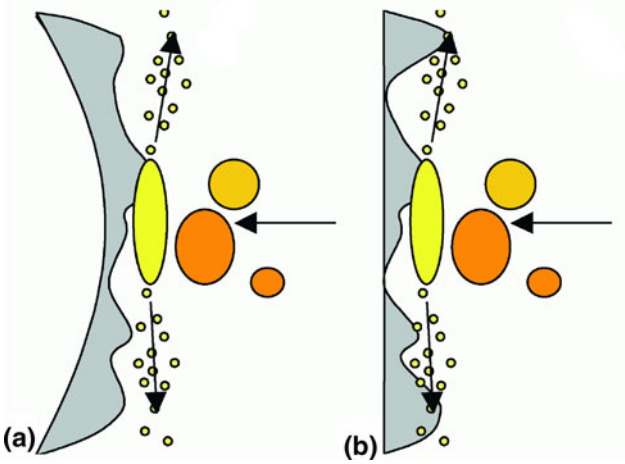

Fig. 15 The relation between the substrate curvature and the suggested speckle formation mechanism; (a) cylindrical and (b) flat surface

protrusion and grew in size progressively with coating deposition forming an approximately conical volume of porosity. This indicates that under certain conditions the growth rate of a speckle was proportional to its size. The porous microstructure was formed by small, sub splat-sized, particles that were highly oxidized. It is hypothesized that droplets or fragments of splashed or fractured particles were responsible for the effect that lead to a speckle formation. Since the trajectories of the splashed particles were more parallel to the substrate particles re-deposited primarily on surfaces inclined to the substrate plane such as the sides of a substrate protrusion, Fig. 4(b). As the speckle or protrusion height over the surrounding coating surface increased the effect was multiplied due to an increased projected area where the splashed particles deposited, Fig. 14. An edge on the surface such as a contact mask would provide an increased projected area for the splashed particles and a microstructure similar to the speckles may form.

The CrC-NiCr coatings sprayed on cylindrical surfaces did not exhibit speckle formation and possessed higher hardness, Fig. 11, and corrosion resistance, Fig. 12. The speckles did not form on the cylindrical surface even at the standoff distance and the flow settings that were associated with speckle formation on the flat specimens. The absence of speckles is in agreement with the suggested mechanism since less splashed particles would be deposited on the cylindrical surface, Fig. 15. Due to the surface curvature of the cylindrical surface, the droplets or fragments would travel higher above the surface and fewer protrusions would extend to their path. Observation of splashed particles collected on polished steel plates also confirmed that the curved surface does not eliminate or mitigate particle splashing but there are fewer particles splashed below the tangent that extends from the point of impact, Fig. 2 and 7.

The same mechanism probably governs the speckle formation on the 316L coatings since speckles occurred at a standoff distance less than 356 mm. Relatively, few speckles were formed on the cylindrical substrate; however, the corrosion resistance appeared unaffected.

Higher particle temperature would be expected at the higher equivalence ratio where the combustion temperature is close to its peak value (Ref 36). However, the in-flight temperature measurements did not indicate a higher particle temperature at a higher equivalence ratio, Fig. 1. This may be a systematic error caused by factors such as: (i) unknown exact particle emissivity at the process temperatures and its changes due to oxidation (ii) emission/absorption from hot gas (Ref 38); however, these effects were not further investigated in the present study. It should be noted that the in-flight diagnostic equipment can measure only the particle surface temperature and particles with different thermal histories and degree of melting may exhibit the same surface temperatures as measured using the in-flight pyrometry (Ref 39). Adjusting the oxygen and fuel mixture to a more lean condition, which would be expected to translate into a colder flame and less melting, resulted in the formation of CrC-NiCr coatings without macro roughness at all standoff distances. Although particle velocity measurement using the in-flight diagnostic equipment may be affected by certain conditions such as too cold particles not being detected (Ref 35), the velocity measurement does not depend on the above-mentioned unknown parameters related to the temperature measurement; therefore, it is assumed that the velocity measurements are relatively correct. Since the average particle velocities under both lean and rich flame conditions, i.e., cold and hot, respectively, were about the same, the splashing behavior was probably governed by the particle viscosity.

It appears that under the low equivalence ratio condition a shorter standoff distance resulted in a more corrosion resistant coating, Fig. 12(a(1-4)). The coating hardness exhibits a similar trend with respect to the standoff distance, Fig. 11, which would be expected since both the corrosion resistance and the mechanical properties such as hardness (Ref 4, 7) and elastic modulus (Ref 6) depend on the coating density.

Speckles were formed within the coatings deposited on the flat specimens at the shorter standoff distances under the high equivalence ratio condition, which had an adverse

effect on the corrosion resistance. The coating deposited on the cylindrical surface under the same conditions possessed, on the other hand, possessed the best resistance to red rust. The results indicate that unless the conditions favor particle splashing the higher the particle kinetic energy the denser coating is formed.

7. Summary

It is important to control the splashing phenomenon during HVOF coating deposition to avoid excessive porosity and oxide content. The splashing can generate macro roughness on the coating surface due to droplet redeposition. The macro roughness features consist of porous material with high oxide content. Surface curvature is an important factor for droplet redeposition; highly curved surfaces tend to mitigate the droplet redeposition effect. Localized porosity that can extend through the coating thickness often originates on small surface asperities such as a residual grit particle. This effect is interesting with respect to macro-roughened surfaces that have been investigated as a way to improve coating adhesion. Particle splashing may affect the coating formation around the protrusions. It is possible that if speckles arranged in an array grow to the extent that they contact each other, further growth would be impeded and smoother coating would be formed on top of the speckles. Particle velocity and temperature are among the factors that have effect on splashing. Particles are typically not fully molten during HVOF processing; however, higher particle temperature results in higher liquid content and lower viscosity. High kinetic energy and low viscosity tends to promote splashing, which is consistent with prior studies of plasma spray processes. Adjusting the process parameters such as flows of the process gases and the standoff distance can effectively control the splashing phenomenon. To better understand the effect of process parameters on splashing, it would be beneficial to determine the degree of particle melting for example by observation of particles trapped in a gel target (Ref 31). Substrate temperature and chemical composition strongly affect the particle deposition and should be investigated in the future studies.

References

1. M.P. Planche, H. Liao, B. Normand, and C. Coddet, Relationships Between NiCrBSi Particle Characteristics and Corresponding Coating Properties Using Different Thermal Spraying Processes, *Surf. Coat. Technol.*, 2005, **200**(7), p 2465-2473
2. D.S. Parker, Case Study: Application of HVOF Sprayed Coatings for Replacement of Chrome Plating on Navy P-3 Aircraft Hydraulic Components and Landing Gear, *Thermal Spray: Meeting the Challenges of the 21st Century*, C. Coddet, Ed., May 25-29, 1998 (Nice, France), ASM International, 1998, p 243-248
3. C. Wasserman, R. Boecking, and S. Gustafsson, Replacement for Hard Chrome Plating in Printing Machinery, *Thermal Spray 2001: New Surfaces for a New Millennium*, C.C. Berndt, Ed., 2001 (Singapore), ASM International, 2001, p 69-74
4. B.Z. Janos, E. Lugscheider, and P. Remer, Effect of Thermal Aging on the Erosion Resistance of Air Plasma Sprayed Zirconia Thermal Barrier Coating, *Surf. Coat. Technol.*, 1999, **113**(3), p 278-285
5. B. Arsenault, J.G. Legoux, H. Hawthorne, J.P. Immarigeon, P. Gougeon, and C. Moreau, HVOF Process Optimization for the Erosion Resistance of WC-12Co and WC-10Co-4Cr Coatings, *Thermal Spray 2001: New Surfaces for a New Millennium*, C.C. Berndt, K.A. Khor, and E.F. Lugscheider, Ed., May 28-30, 2001 (Singapore), ASM International, 2001, p 1051-1060
6. F. Kroupa and J. Dubsky, Pressure Dependence of Young's Moduli of Thermal Sprayed Materials, *Scripta Mater.*, 1999, **40**(11), p 1249-1254
7. T.P. Hoepfner and E.D. Case, The Influence of the Microstructure on the Hardness of Sintered Hydroxyapatite, *Ceram. Int.*, 2003, **29**(6), p 699-706
8. H.A. Jehn and A. Zielonka, Corrosion Testing, *ASM Handbook, Volume 5 Surface Engineering*, S.R. Lampman, Ed., ASM International, Materials Park, OH, 1994, p 635-641
9. J. Kawakita, S. Kuroda, T. Fukushima, and T. Kodama, Development of Dense Corrosion Resistant Coatings by an Improved HVOF Spraying Process, *Sci. Technol. Adv. Mater.*, 2003, **4**(4), p 281-289
10. T.C. Totemeier, Effect of High-Velocity Oxygen-Fuel Thermal Spraying on the Physical and Mechanical Properties of Type 316 Stainless Steel, *J. Therm. Spray. Technol.*, 2005, **14**(3), p 369-372
11. D.T. Gawne, B.J. Griffiths, and G. Dong, Splat Morphology and Adhesion of Thermally Sprayed Coatings, *Thermal Spraying: Current Status and Future Trends*, A. Ohmori, Ed., May 22-26, 1995 (Kobe, Japan), High Temperature Society of Japan, 1995, p 779-784
12. A.P. Newbery and P.S. Grant, Droplet Splashing During Arc Spraying of Steel and the Effect on Deposit Microstructure, *J. Therm. Spray Technol.*, 2000, **9**(2), p 250-258
13. R.W. Trice and K.T. Faber, Role of Lamellae Morphology on the Microstructural Development and Mechanical Properties of Small-Particle Plasma-Sprayed Alumina, *J. Am. Ceram. Soc.*, 2000, **83**(4), p 889-896
14. C. Mundo, M. Sommerfeld, and C. Tropea, Droplet-Wall Collisions: Experimental Studies of the Deformation and Breakup Process, *Int. J. Multiphas. Flow*, 1995, **21**(2), p 151-173
15. M. Bussmann, S.D. Aziz, S. Chandra, and J. Mostaghimi, 3D Modelling of Thermal Spray Droplet Splashing, *Thermal Spray: Meeting the Challenges of the 21st Century*, C. Coddet, Ed., 1998 (Nice, France), ASM International, 1998, p 413-418
16. X. Jiang, J. Matejicek, and S. Sampath, Substrate Temperature Effects on the Splat Formation, Microstructure Development and Properties of Plasma Sprayed Coatings Part II: Case Study for Molybdenum, *Mater. Sci. Eng. A*, 1999, **272**(1), p 189-198
17. P. Fauchais, M. Fukumoto, A. Vardelle, and M. Vardelle, Knowledge Concerning Splat Formation: An Invited Review, *J. Therm. Spray Technol.*, 2004, **13**(3), p 337-360
18. M. Fukumoto, S. Katoh, and I. Okane, Splat Behavior of Plasma Sprayed Particles on Flat Substrate Surface, *Thermal Spraying: Current Status and Future Trends*, A.P.O. Ohmori, Ed., May, 1995 (Kobe, Japan), The Society, 1995, p 353-358
19. M. Fukumoto, Y. Huang, and M. Ohwatari, Flattening Mechanism in Thermal Sprayed Particle Impinging on Flat Substrate, *Thermal Spray: Meeting the Challenges of the 21st Century*, C. Coddet, Ed., 1998 (Nice, France), ASM International, 1998, p 401-406
20. M. Fukumoto, E. Nishioka, and T. Matsubara, Effect of Interface Wetting on Flattening of Freely Fallen Metal Droplet onto Flat Substrate Surface, *J. Therm. Spray Technol.*, 2002, **11**(1), p 69-74
21. L. Bianchi, A.C. Leger, M. Vardelle, A. Vardelle, and P. Fauchais, Splat Formation and Cooling of Plasma-Sprayed Zirconia, *Thin Solid Films*, 1997, **305**(1-2), p 35-47
22. C. Moreau, M. Lamontagne, and P. Cielo, Influence of the Coating Thickness on the Cooling Rate of Plasma-Sprayed Particles Impinging on a Substrate, *Thermal Spray Coatings: Properties, Processes and Applications*, T.F. Bernecki, Ed., May 4-10, 1991 (Pittsburgh, PA), 1991, p 237-243
23. M. Fukumoto, E. Nishioka, and T. Nishiyama, Proposal of New Criterion for Splashing of Thermal Sprayed Particle onto Flat Substrate Surface, *Thermal Spray 2001: New Surfaces for a*

New Millennium, C.C. Berndt, Ed., 2001 (Singapore), ASM International, 2001, p 841-848
24. Y.Y. Wang, C.J. Li, and A. Ohmori, Influence of Substrate Roughness on the Bonding Mechanisms of High Velocity Oxy-Fuel Sprayed Coatings, *Thin Sol. Films*, 2005, **485**(1-2), p 141-147
25. C. Moreau, P. Gougeon, and M. Lamontagne, Influence of Substrate Preparation on the Flattening and Cooling of Plasma-Sprayed Particles, *J. Therm. Spray Technol.*, 1995, **4**(1), p 25-33
26. A. McDonald, S. Chandra, and C. Moreau, Photographing Impact of Plasma-Sprayed Particles on Rough Substrates, *J. Mater. Sci.*, 2008, **43**(13), p 4631-4643
27. J. Cedelle, M. Vardelle, and P. Fauchais, Influence of Stainless Steel Substrate Preheating on Surface Topography and on Millimeter- and Micrometer-Sized Splat Formation, *Surf. Coat. Technol.*, 2006, **201**(3-4), p 1373-1382
28. M. Fukumoto, T. Yamaguchi, M. Yamada, and T. Yasui, Splash Splat to Disk Splat Transition Behavior in Plasma-Sprayed Metallic Materials, *J. Therm. Spray Technol.*, 2007, **16**(5-6), p 905-912
29. X. Jiang, Y. Wan, H. Herman, and S. Sampath, Role of Condensates and Adsorbates on Substrate Surface on Fragmentation of Impinging Molten Droplets During Thermal Spray, *Thin Solid Films*, 2001, **385**(1-2), p 132-141
30. A. Abedini, A. Pourmousa, S. Chandra, and J. Mostaghimi, Effect of Substrate Temperature on the Properties of Coatings and Splats Deposited by Wire Arc Spraying, *Surf. Coat. Technol.*, 2006, **201**(6), p 3350-3358
31. H. Yamada, S. Kuroda, T. Fukushima, and H. Yumoto, Capture and Evaluation of HVOF Thermal Sprayed Particles by a Gel Target, *Thermal Spray 2001: New Surfaces for a New Millennium*, C.C. Berndt, Ed., 2001 (Singapore), ASM International, 2001, p 797-804
32. W. Trompetter, M. Hyland, D. McGrouther, P. Munroe, and A. Markwitz, Effect of Substrate Hardness on Splat Morphology in High-Velocity Thermal Spray Coatings, *J. Therm. Spray Technol.*, 2006, **15**(4), p 663-669
33. E. Strock, P. Ruggiero, and D. Reynolds, The Effect of Off-Angle Spraying on the Structure and Properties of HVOF WC/CoCr Coatings, *Thermal Spray 2001: New Surfaces for a New Millennium*, C.C. Berndt, Ed., 2001 (Singapore), ASM International, 2001, p 671-676
34. W. Tillmann, E. Vogli, and B. Krebs, Influence of the Spray Angle on Characteristics for Atmospheric Plasma Sprayed Hard Material Based Coatings, *Thermal Spray 2008: Thermal Spray Crossing Borders*, E. Lugscheider, Ed., 2008 (Maastricht, NL), DVS—German Welding Society, 2008, p 247-252
35. J.F. Bisson, M. Lamontagne, C. Moreau, L. Pouliot, J. Blain, and F. Nadeau, Ensemble In-Flight Particle Diagnostics under Thermal Spray Conditions, *Thermal Spray 2001: New Surfaces for a New Millennium*, C.C. Berndt, K.A. Khor, and E.F. Lugscheider, Ed., May 28-30, 2001 (Singapore), ASM International, 2001, p 705-714
36. C.K. Law, A. Makino, and T.F. Lu, On the Off-Stoichiometric Peaking of Adiabatic Flame Temperature, *Combust. Flame*, 2006, **145**(4), p 808-819
37. W.C. Oliver and G.M. Pharr, An Improved Technique for Determining Hardness and Elastic-Modulus Using Load and Displacement Sensing Indentation Experiments, *J. Mater. Res.*, 1992, **7**(6), p 1564-1583
38. C. Kerr and P. Ivey, An Overview of the Measurement Errors Associated with Gas Turbine Aeroengine Pyrometer Systems, *Meas. Sci. Technol.*, 2002, **13**(6), p 873-881
39. R. Molz, A. Valarezo, and S. Sampath, Comparison of Coating Stresses Produced by High Velocity Liquid/Gas Fuel and Triplex Pro 200 Plasma Processes Using In Situ Coating Stress Measurement, *Thermal Spray 2008: Thermal Spray Crossing Borders*, E. Lugscheider, Ed., 2008 (Maastricht, NL), DVS—German Welding Society, 2008, p 473-478